BRAIN
ORIGINAL ARTICLE

Downregulation of PMP22 ameliorates myelin defects in iPSC-derived human organoid cultures of CMT1A

Jonas Van Lent,[1,2] Leen Vendredy,[1,2] Elias Adriaenssens,[1,2] Tatiana Da Silva Authier,[1,2] Bob Asselbergh,[3,4] Marcus Kaji,[5] Sarah Weckhuysen,[5,6,7] Ludo Van Den Bosch,[8,9] Jonathan Baets[2,10] and Vincent Timmerman[1,2]

Charcot–Marie–Tooth disease is the most common inherited disorder of the PNS. CMT1A accounts for 40–50% of all cases and is caused by a duplication of the *PMP22* gene on chromosome 17, leading to dysmyelination in the PNS. Patient-derived models to study such myelination defects are lacking as the *in vitro* generation of human myelinating Schwann cells has proved to be particularly challenging. Here, we present an induced pluripotent stem cell-derived organoid culture, containing various cell types of the PNS, including myelinating human Schwann cells, which mimics the human PNS. Single-cell analysis confirmed the PNS-like cellular composition and provides insight into the developmental trajectory. We used this organoid model to study disease signatures of CMT1A, revealing early ultrastructural myelin alterations, including increased myelin periodic line distance and hypermyelination of small axons. Furthermore, we observed the presence of onion-bulb-like formations in a later developmental stage. These hallmarks were not present in the CMT1A-corrected isogenic line or in a CMT2A iPSC line, supporting the notion that these alterations are specific to CMT1A. Downregulation of *PMP22* expression using short-hairpin RNAs or a combinatorial drug consisting of baclofen, naltrexone hydrochloride and D-sorbitol was able to ameliorate the myelin defects in CMT1A-organoids. In summary, this self-organizing organoid model can capture biologically meaningful features of the disease and capture the physiological complexity, forms an excellent model for studying demyelinating diseases and supports the therapeutic approach of reducing *PMP22* expression.

1 Peripheral Neuropathy Research Group, Department of Biomedical Sciences, University of Antwerp, Antwerp 2610, Belgium
2 Laboratory of Neuromuscular Pathology, Institute Born Bunge, and Translational Neurosciences, Faculty of Medicine, University of Antwerp, Antwerp 2610, Belgium
3 Neuromics Support Facility, VIB Center for Molecular Neurology, VIB, Antwerp 2610, Belgium
4 Neuromics Support Facility, Department of Biomedical Sciences, University of Antwerp, Antwerp 2610, Belgium
5 Applied & Translational Neurogenomics Group, VIB Center for Molecular Neurology, VIB, University of Antwerp, Antwerp 2610, Belgium
6 Department of Neurology, Antwerp University Hospital, Antwerp 2610, Belgium
7 Translational Neurosciences, Faculty of Medicine and Health Science, University of Antwerp, Antwerp 2610, Belgium
8 Department of Neurosciences, Experimental Neurology, Leuven Brain Institute, KU Leuven—University of Leuven, Leuven 3000, Belgium
9 VIB-Center for Brain & Disease Research, Laboratory of Neurobiology, Leuven 3000, Belgium
10 Neuromuscular Reference Centre, Department of Neurology, Antwerp University Hospital, Antwerp 2610, Belgium

Received April 01, 2022. Revised November 23, 2022. Accepted November 27, 2022. Advance access publication December 13, 2022

Correspondence to: Professor Dr Vincent Timmerman, PhD
Peripheral Neuropathy Research Group
University of Antwerp, Universiteitsplein 1
BE-2610, Antwerpen, Belgium
E-mail: vincent.timmerman@uantwerpen.be

Keywords: Charcot–Marie–Tooth neuropathy; iPSC-derived PNS organoid cultures; myelinating Schwann cells; short-hairpin RNAs targeting PMP22; combinatorial drug (baclofen; naltrexone hydrochloride and D-sorbitol)

Introduction

Charcot–Marie–Tooth (CMT) disease or hereditary motor and sensory neuropathy affects the PNS and results in progressive distal muscle weakness and loss of sensation in the lower and upper limbs. CMT is divided in two main subtypes, demyelinating CMT1 and axonal CMT2, depending on whether the underlying genetic cause primarily affects myelinating Schwann cells or peripheral nerve axons.[1]

The most common form of CMT is CMT1A, representing 40–50% of all CMT patients and about two-thirds or more of demyelinating CMT cases. It is caused by a tandem duplication of a 1.4 Mbp region on chromosome 17p11.2-p12, containing the peripheral myelin protein 22 gene (*PMP22*).[2–4] This duplication leads to an increased dosage of PMP22 expression, thereby disturbing the myelination process. As a consequence, typical hallmarks of CMT1A patients include complex dysmyelination and onion-bulb formations that can be diagnosed on nerve biopsies.[5]

Induced pluripotent stem cells (iPSCs) form a powerful tool to study CMT with.[6,7] Different studies reported CMT disease hallmarks in e.g. iPSC-derived motor or sensory neuron cultures.[8–10] However, the complex process of myelination cannot be mimicked by such monocultures, as myelination involves a well-organized and structured wrapping of neurons by Schwann cells. Therefore, the *in vitro* formation of such PNS models would require the presence of multiple cell types in the same dish. Attempts to study demyelinating diseases *in vitro* have so far relied on co-cultures between iPSC-derived neurons and myelinating Schwann cells from rats.[11] Although Schwann cells have been successfully differentiated from iPSCs,[12] they fail to robustly myelinate iPSC-derived neurons *in vitro*, similarly to primary human Schwann cells. A major step forward to allow further developments in this field would be the establishment of a human model for the PNS that includes myelinating Schwann cells, but also other relevant cell types such as muscle cells, to which neurons need to connect to form functional neuromuscular junctions (NMJs). To overcome existing hurdles, creating human iPSC-organoid models is a promising strategy.

Even though CMT is the most common inherited peripheral neuropathy, the disease remains incurable. The largest clinical trial for CMT to date was performed for the CMT1A duplication, in which ascorbic acid treatment was evaluated and found unable to improve the course of the neuropathy, despite promising preclinical results in CMT1A rodent models. While this underscored the need for improved human model systems, new clinical trials for CMT1A have been initiated and are currently ongoing. The most progressed candidate therapies are PXT3003, a combinatorial drug currently in clinical trial Phase III, which was shown to reduce *PMP22* expression,[13,14] and antisense oligonucleotides (ASO)[15] plus RNA-interference (RNAi) approaches[16,17] that directly inhibit PMP22 expression.

Here we report the development of a human iPSC-derived organoid model, that contains neurons, muscle cells, Schwann cells, endothelial and glial cells. With the presence of myelinated neurons and NMJs, the organoid captures key features of the PNS. Moreover, organoids generated from CMT1A showed that hallmarks of the disease are recapitulated. Treatment of the CMT1A-organoids revealed that myelin defects can be rescued. Together, we describe an organoid model that can be used to investigate peripheral neuropathies, and we highlight its therapeutic potential.

Materials and methods

Induced pluripotent stem cell lines and maintenance

Human iPSC lines include a healthy unrelated control along with a CMT1A (PMP22 duplication) patient line (CS67iCMT, obtained from Cedars-Sinai Biomanufactoring Center iPSC Core Repository), corresponding TALEN-corrected isogenic line ($CMT1A^{ISO}$) and a CMT2A (c.281G>A, R94Q) patient line, which were all previously described (Supplementary Table 1). The iPSC lines were cultured and maintained on Matrigel coated plates (734–1440, VWR biotechnologies) in Essential 8 Flex medium and supplement (A2858501, Thermo Fisher).[8] RevitaCell supplement (A2644501, Thermo Fisher) was used to enhance cell survival on reviving. Medium was refreshed every alternate day and iPSCs were passaged using Versene (EDTA) (LO BE17-711E, Westburg). All the iPSC lines were tested negative for *Mycoplasma*. All experiments with patient material were approved by the Committee for Medical Ethics, University of Antwerp.

Differentiation of induced pluripotent stem cells into organoids

Differentiation of iPSCs into organoids was adapted from a previously published protocol.[18] Briefly, iPSC colonies were enzymatically dissociated using StemPro Accutase Cell Dissociation Reagent (A1110501, Thermo Fisher), when 80% confluency was reached. At Day 0, single cells were resuspended in organoid medium consisting of STEMdiff APEL2 Medium (05270, Stemcell Technologies) and 5.32% Protein Free Hybridoma Medium II (12040077, Thermo Fisher) supplemented with 0.5 µM CHIR99021 (CHIR, 4423/10, Bio-Techne), 10 ng/ml basic fibroblast growth factor (bFGF, 233-FB-025, Bio-Techne), 20 µM Forskolin (sc-3562, Santa Cruz Biotechnology) and 10 µM ROCK Inhibitor (Y-27632) (688001-500, VWR biotechnologies). Single cells were plated at a density of 300 000 cells/ml on an AggreWell 800 plate (34811, Stemcell Technologies) that was pretreated with an Anti-Adherence Rinsing Solution (07010, Stemcell Technologies). Afterwards, the plate was centrifuged at 100*g* for 3 min. The

medium was changed every day, however, on the first day only 30% of the organoid medium was added with a 3-fold increase in the concentrations of the supplements. After 1 week, spheres were collected and replated in ultra-low binding 96-well plates (7007, Corning). Plates were kept on an orbital shaker (KS 260 control, IKA) at 70 rpm and from Day 9 onwards, half of the medium was replaced with Dulbecco's modified Eagle medium, high glucose (41965039, Thermo Fisher) containing 2% horse serum (16050130, Thermo Fisher). After 2 weeks, the organoids were transferred into Matrigel to further develop and mature.

Electron microscopy

For transmission electron microscopy (TEM), organoids were fixed in 2.5% glutaraldehyde containing solution. Afterwards, organoids were embedded in 2% low-melting point agarose for further processing. Next, three washes in 0.1 M sodium cacodylate buffer (pH 7.4), containing 7.5% saccharose, were performed. Post-fixation was performed by incubating cells for 2 h with 1% OsO_4 solution. After dehydration in an ethanol gradient, samples were embedded in EM-bed812.

Ultrathin sections were stained with lead citrate, and examined in a Tecnai G2 Spirit Bio TWIN microscope (Fei, Europe BV) at 120 kV. Quantification of the periodic line distance and the *g*-ratio was performed with randomly selected neurons using the Fiji distribution of ImageJ.[19,20] The *g*-ratio was quantified as the ratio between the axon diameter (major axis) and the fibre diameter. To analyse the periodic line distance, straight lines were drawn across myelin sheaths. The average periodic distance was calculated from at least three periodic distances per myelinated neuron. For scanning electron microscopy, organoids were Matrigel-embedded on coverslips and fixed afterwards in 2.5% glutaraldehyde solution in 0.1 M sodium cacodylate buffer (pH 7.4). After dehydration in an ethanol gradient (50–70–90–95–100% ethanol), samples were critical point dried, mounted on a scanning electron microscope grid and sputter coated with 20 nm gold particles. Images were recorded with a JSM-IT100 scanning electron microscope (Jeol). The post-mortem sural nerve biopsy was studied in a CMT1A patient at the age of 73 years. The nerve was fixed in 4.5% phosphate-buffered glutaraldehyde, post-fixed in 2% phosphate-buffered osmium tetroxide and embedded in Araldite. Ultrathin sections were stained with uranyl acetate and lead citrate and were examined with a Philips CM10 electron microscope at 60 kV.

Short-hairpin RNAs targeting PMP22

Short-hairpin RNAs (shRNAs) of the Sigma Mission pLKO.1-library were obtained from BCCM/GeneCorner Plasmid Collection (https://bccm.belspo.be/). Two shRNAs against human PMP22 (TRCN0000082803 and TRCN0000082805) were used in this study, in addition to a non-mammalian shRNA control (SH002) (Supplementary Table 4).

Lentiviral transduction was used to stably express the previously mentioned shRNAs. To this end, human embryonic kidney 293T cells were transiently transfected with packaging (pCMV dR8.91), envelope (pMD2-VSV) and pLKO.1 plasmids using PEI MAX 40K transfection agent (24765-1, PolySciences Europe). After 48 h, virus containing supernatant was collected from human embryonic kidney 293T cells, filtered through a 0.45 μm filter (SLHV033RB, Millipore) and concentrated using an Amicon Ultra-15 Centrifugal Filter Unit (UFC905024, Millipore). The lentiviral titre was quantified using Lenti-X GoStix Plus (631280, Takara Bio) (Supplementary Table 5). Snap-frozen aliquots were thawed just before transducing early organoids (D7) and added in low (25 μl) and high (75 μl) concentrations (Supplementary Table 5). Virus containing medium was removed 48 h after transduction and replaced by D9 differentiation medium.

Combinatorial drug treatment

Organoids were treated with a combinatorial drug from Day 6 onwards, consisting of 25 nM (±)-baclofen (B5399), 3 nM naltrexone hydrochloride (N3136) and 800 nM D-sorbitol (S3889), all obtained from Sigma-Aldrich. An equivalent amount of DMSO was used as a vehicle.

Statistical analysis

All experiments were performed in independent differentiations (except single-cell RNA-seq). Statistical analysis was performed using GraphPad Prism (v.8.3.1). Normality was tested using the Shapiro–Wilk test, followed by the Mann–Whitney U-test (not normally distributed) comparing two groups. Data containing three groups were analysed with either a one-way ANOVA followed by Tukey's multiple comparisons test (normal distribution) or a Kruskal–Wallis non-parametric test with Dunn's correction for multiple comparisons. $^{*}P < 0.05$, $^{**}P < 0.01$, $^{***}P < 0.001$, $^{****}P < 0.0001$ were considered significant. Data values represented mean ± standard error of the mean (SEM), except otherwise mentioned.

Data availability

The generated data are available from the corresponding author upon reasonable request.

Results

Characterization of self-organizing induced pluripotent stem cell-derived organoids

Since traditional 2D cultures cannot capture the full physiological complexity of the human PNS, we set out to develop a novel organoid-based model adapted from a previously established protocol (Fig. 1A).[18] We dissociated iPSCs into single cells and replated them into microwells, supplemented with bFGF, CHIR and Forskolin for 7 days. At Day 2, the cells became neuromesodermal progenitors, expressing both SOX2 and T/BRA (Fig. 1B). These cells gave rise to neuroectodermal and mesodermal cell derivatives.[18,21,22] After 1 week, cells were transferred to ultra-low attachment plates on an orbital shaker, where the medium was gradually changed to high-glucose Dulbecco's modified Eagle medium, containing 2% horse serum. After 2 weeks, organoids were embedded in Matrigel to allow further maturation.

To determine the composition of healthy control organoids, we performed single-cell RNA-sequencing at Day 2 and Day 20. We analysed the transcriptomes of 25 965 cells from Day 2 cultures using microfluidic inDrop single-cell RNA-sequencing, with a mean of 14 769 reads/cell (Supplementary Fig. 1A–C). At this early stage of differentiation, populations of ribosomal and mitochondrial marker genes were detected, playing a crucial role in early developmental processes (clusters 1, 4). The remaining transcript profiles (clusters 2, 3) contained marker genes characteristic for both neuroectodermal development as well as mesodermal development (such as *SOX2*, *TUBB2B*, *PAX6*, *FOXC1* and *SOX9*).[22]

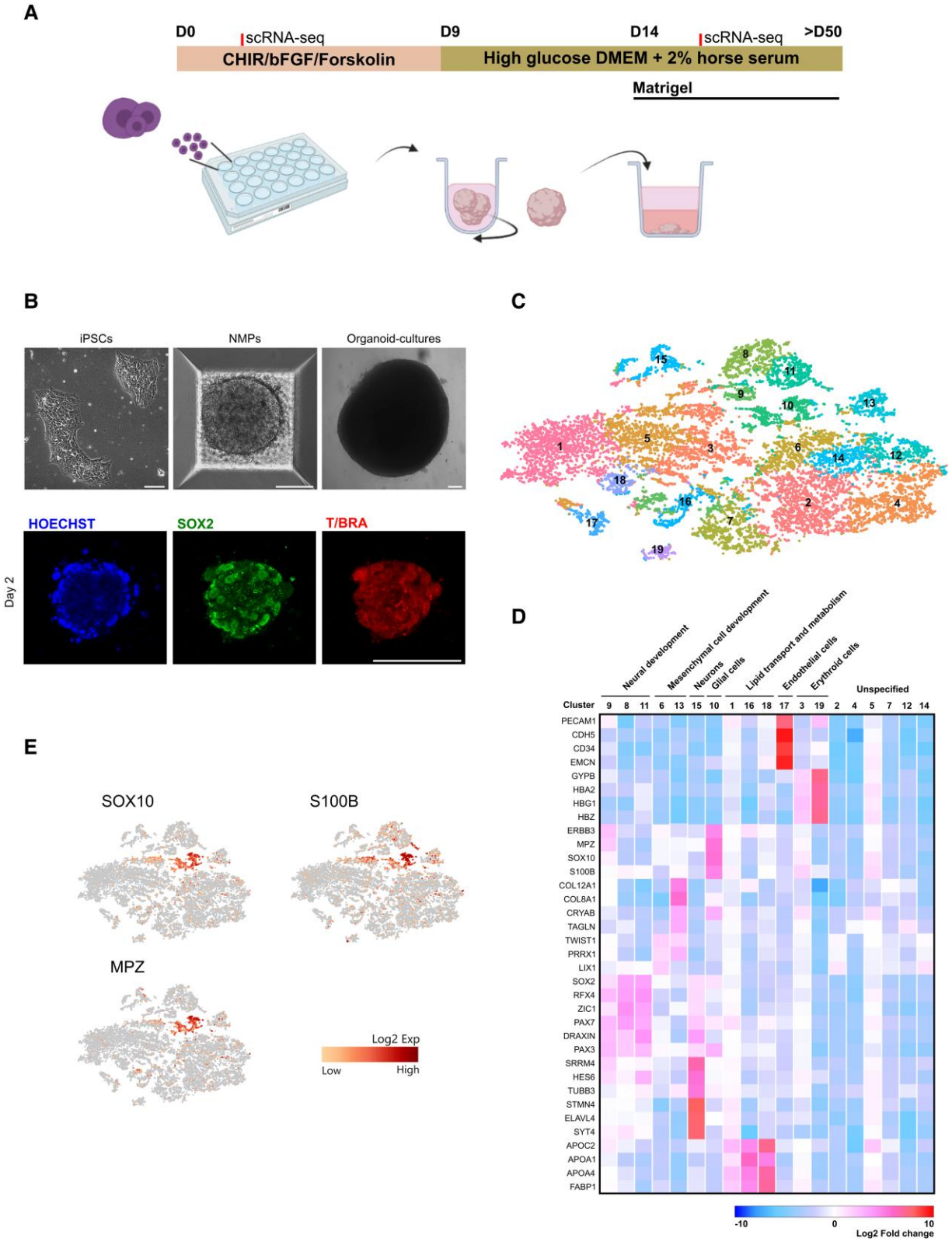

Figure 1 Generation and transcriptional characterization of iPSC-derived organoid cultures. (**A**) Graphic scheme of procedures for the generation of iPSC-derived organoid cultures. The iPSCs were dissociated in single cells and aggregated in microwells. Cells were transferred into an ultra-low attachment plate on an orbital shaker, and afterwards grown as 3D cultures in Matrigel. *Top*: compounds used to obtain organoid cultures. CHIR = CHIR99021; bFGF = basic fibroblast growth factor; DMEM = Dulbecco's modified Eagle medium; NMP = neuromesodermal progenitor. Figure created with BioRender. (**B**) Phase contrast images of the different stages. Immunostainings at Day 2 of SOX2, T/BRA and DNA (Hoechst 33342). Scale bar = 100 µm. (**C**) *t*-distributed stochastic neighbour embedding plot of control organoid at Day 20. Individual cells are visualized as dots and clusters of cells as coloured groups, along with the corresponding cluster numbers. (**D**) Heat map of cluster-defining marker genes of main identified cell populations. Clusters that could not be unambiguously identified with broad cell types are labelled as unspecified. Log2 Fold change, Red (+10 at the *right* end): high expression, blue (−10 at the *left* end): low/no expression. (**E**) Expression of specific genes, i.e. SOX10, S100B and MPZ, displayed on *t*-distributed stochastic neighbour embedding maps. Orange = high expression; grey = low/no expression.

We also determined the composition of more matured organoids at Day 20, where 14 040 cells were analysed with a mean of 57 078 reads/cell. Cells were clustered into 19 independent groups (Fig. 1C). The cluster identity was assessed using differentially expressed cluster marker genes (Fig. 1D). The neuroectodermal and mesodermal progenitor cells, detected at the early time point, further expanded into a heterogeneous organoid model. Marker genes revealed seven broad cell populations discriminating cells involved in neural development (clusters 9, 8, 11) defined by expression of marker genes such as *SOX2*, *DRAXIN* and *RFX4*,[18,23,24] mesenchymal cell development (clusters 6, 13) defined by the presence of *TWIST1* and *PRRX1* marker genes[18] as well as collagen marker genes, neurons (cluster 15), glial cells (cluster 10), cells involved in lipid transport and metabolism (clusters 1, 16, 18) identified by expression of marker genes such as *APOA1*, *APOC2* and *FABP1*,[25] endothelial cells (cluster 17) and erythroid cells (clusters 3, 19). We also detected *SOX10*, *S100B* and *MPZ* (cluster 10) (Fig. 1E), genes known to be important throughout Schwann cell development.[26,27] On the contrary, oligodendrocyte marker genes *MOG* and *MOBP* were not detected (Supplementary Fig. 1D). The organoids therefore represent the main PNS cell types also detected by single-cell analysis of mice peripheral nerves.[27]

Organoids contain neuromuscular junctions and myelinating Schwann cells

To further confirm the simultaneous development of ectodermal and mesodermal derived cell types within healthy control organoids, we performed whole mount immunostainings. This revealed the presence of Islet1-positive peripheral neurons (Supplementary Fig. 2A). Mesoderm-derived endothelial and muscle cells were also detected, visualized using either tomato lectin (Supplementary Fig. 2A) or marked as desmin-positive cells (Supplementary Fig. 2B), respectively.

As both neurons and muscle cells developed simultaneously, we verified whether they formed functional neuromuscular connections using α-bungarotoxin (αBTX). This indeed revealed the formation of NMJs (Supplementary Fig. 2B). Using electron microscopy, we also detected synaptic vesicles in the presynaptic nerve terminal (Supplementary Fig. 2C), indicative of functional neuromuscular units.

In addition to the neuromuscular cell types, we also detected glial fibrillary acidic protein, a glial marker and a range of Schwann cell markers important throughout development, such as: myelin protein zero (MPZ, also called P0), myelin basic protein (MBP) and S100 (Fig. 2A and Supplementary Fig. 3A). These results confirm the presence of both glial and Schwann cells. In addition, quantitative polymerase chain reaction with reverse transcription (RT–qPCR) demonstrated an increase in relative expression of *MBP* over time from iPSC colonies (Day 0) to mature organoid cultures (Fig. 2B). TEM confirmed the presence of myelinating Schwann cells and the development of myelin compaction (Fig. 2C), while the typical spindle-elongated morphology of Schwann cells was revealed by scanning electron microscopy (Fig. 2D).

Next, we performed multi-electrode array (MEA) experiments to assess their electrophysiological properties. Organoids were plated on high-density MEA plates and the medium was gradually shifted to BrainPhys™ Neuronal medium containing 2% horse serum. Three weeks after plating the organoids, we observed spontaneous spiking and synchronized network burst electrical activity (Fig. 2E). Owing to the high density of the electrodes, we were able to follow the spatial-temporal propagation of action potentials along neuronal axons and use this to measure the conduction velocity (Fig. 2F). In contrast to unmyelinated neurons, where the action potential travels continuously along the axons, we observed non-continuous conduction velocities along axons, which would be indicative of myelinated sections and suggest the presence of saltatory conduction.[28]

Together, these experiments show that this *in vitro* model mimics the cell type diversity of the PNS and that the model can recapitulate complex interactions between different cell types, such as those required to form myelinated axons.

Organoids from CMT1A patients demonstrate alterations in myelination characteristics

As we successfully generated myelinating human Schwann cells within an organoid model, we tested whether these organoids are suitable to study CMT1A.

We differentiated iPSCs from a healthy control, an axonal CMT2A patient, a demyelinating CMT1A patient and the corresponding corrected isogenic CMT1A^{ISO} control. We observed no differences between the different cell lines when stained for the previously described cell types at the iPSC-stage, neuromesodermal progenitors or differentiated organoids (Supplementary Fig. 3). This shows that none of the cell lines has inherent differentiation defects, permitting us to pursue a deeper characterization of the different lines.

To verify whether we can detect disease-associated defects in the organoids, we analysed the myelin sheath thickness in the CMT1A organoid at Day 25 and compared it to the healthy control. The model contained mostly small axons (<1 µm), possibly indicating it recapitulates the early developmental stages. The comparison of the CMT1A organoids with CMT2A and healthy control organoids revealed hypermyelination of the smallest axons in CMT1A, as shown by their decreased *g*-ratio (Fig. 3A). In addition, we found an increased myelin periodic line distance in CMT1A (Fig. 3B), similar to what is observed in sural nerves from CMT1A patients[29] and in CMT1A rodents.[17]

At a later developmental stage we also recognized onion-bulb-like formation in the CMT1A organoid (Fig. 3C). This is a well-known hallmark of Schwann cell pathology in demyelinating neuropathies. To illustrate this pathological feature, we added an archived post-mortem sural nerve biopsy of a genetically confirmed CMT1A patient at the age of 73 years (Fig. 3D). These structures were not observed in control or CMT2A organoids. Combined, our data show that organoid cultures for CMT1A recapitulate key features of the myelin pathology in humans.

Correction of the CMT1A duplication restores disease phenotypes

To investigate whether correcting the duplication would restore the characteristic disease phenotypes, we performed organoid differentiations of a for CMT1A corrected isogenic iPSC line (CMT1A^{ISO}).[30] To investigate the *PMP22* gene dosage difference, we measured *PMP22* expression levels at Day 25, which were found to be increased in the CMT1A line compared to the corrected CMT1A^{ISO} line (Fig. 4A).

Since imbalanced activity of the PI3K-Akt signalling pathway has been identified as an early characteristic of CMT1A, causing perturbed Schwann cell differentiation,[13,31] we determined p-Akt/Akt ratios in the CMT1A organoids and observed a reduced p-Akt/Akt ratio compared to the isogenic CMT1A^{ISO} line (Fig. 4B).

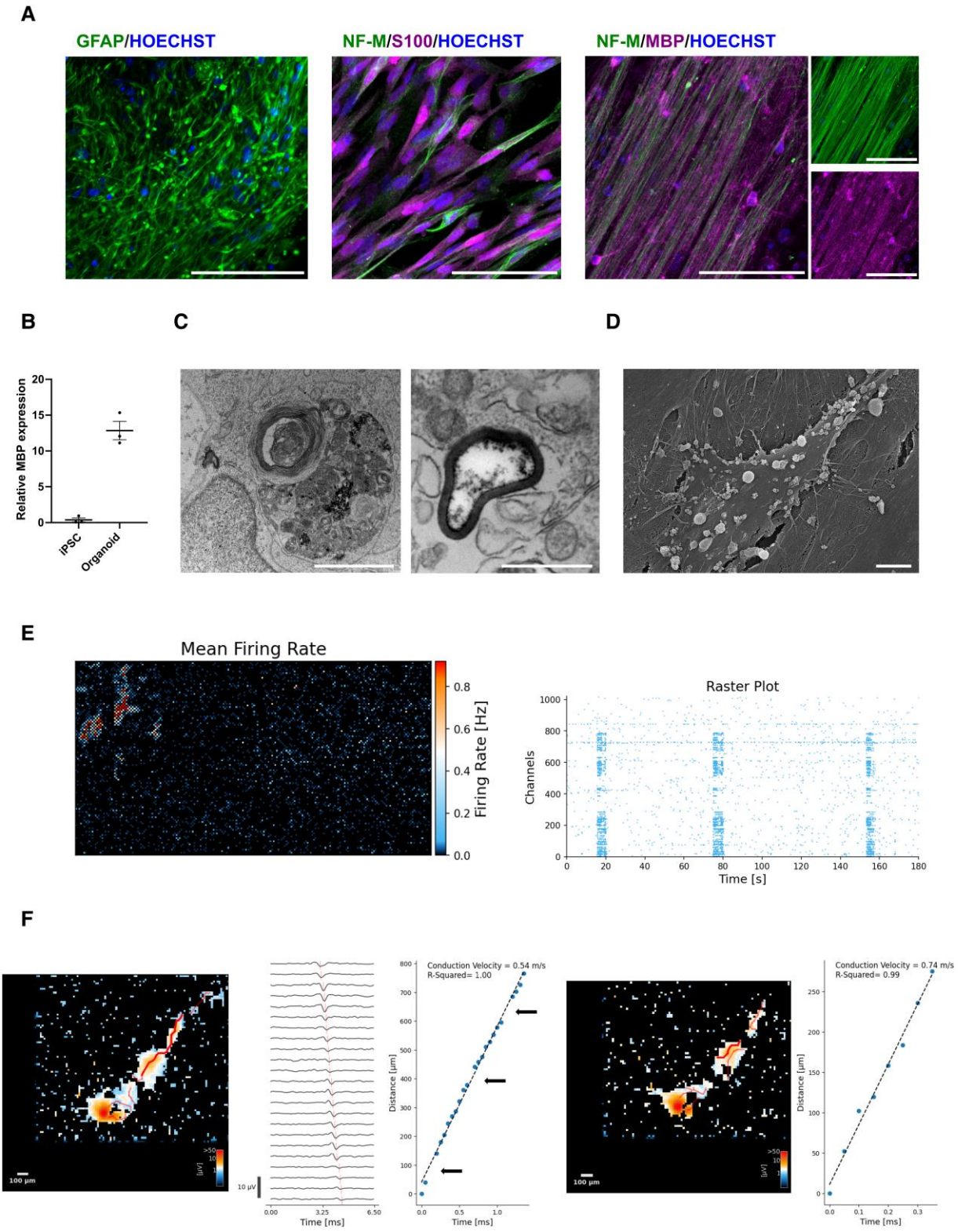

Figure 2 Characterization of myelinated neurons in organoid cultures. (**A**) Immunostainings at Day 50 with glial fibrillary acidic protein (GFAP) (glial cells), NF-M (neurofilament), S100 (Schwann cells), MBP (myelin) and Hoechst 33342. These stainings indicate that S100-positive Schwann cells and MBP are aligned with neurofilaments. Scale bar = 100 µm. (**B**) RT-qPCR to investigate the relative expression of *MBP* in iPSC colonies at Day 0, and at mature organoid stages *in vitro* ($n = 3$; data pooled from two independent differentiations; mean ± SEM). (**C**) TEM images at Day 18 of Schwann cell with (partially) uncompacted myelin (*left*) and with compact myelin (*right*). Scale = 500 nm. (**D**) Scanning electron microscopy image at Day 50 of Schwann cell with spindle-elongated morphology. Scale bar = 5 µm. (**E**) MEA activity analysis of organoids, 3 weeks after plating. Spontaneous extracellular action potential (spikes) and network burst electrical activity were observed. (**F**) MEA axonal action potential propagation tracking was performed to measure the axon conduction velocity. The red bold selected branch and its corresponding action potentials are displayed. Arrows indicate the longer time taken for the action potential to transverse a certain distance (*left*). A separate footprint of the same neuron, covering a tracked region of the selected branch showing a higher conduction velocity (*right*). Statistical significance of RT-qPCR results was calculated using the Mann–Whitney U-test (*$P < 0.05$, **$P < 0.01$, ***$P < 0.001$, ****$P < 0.0001$).

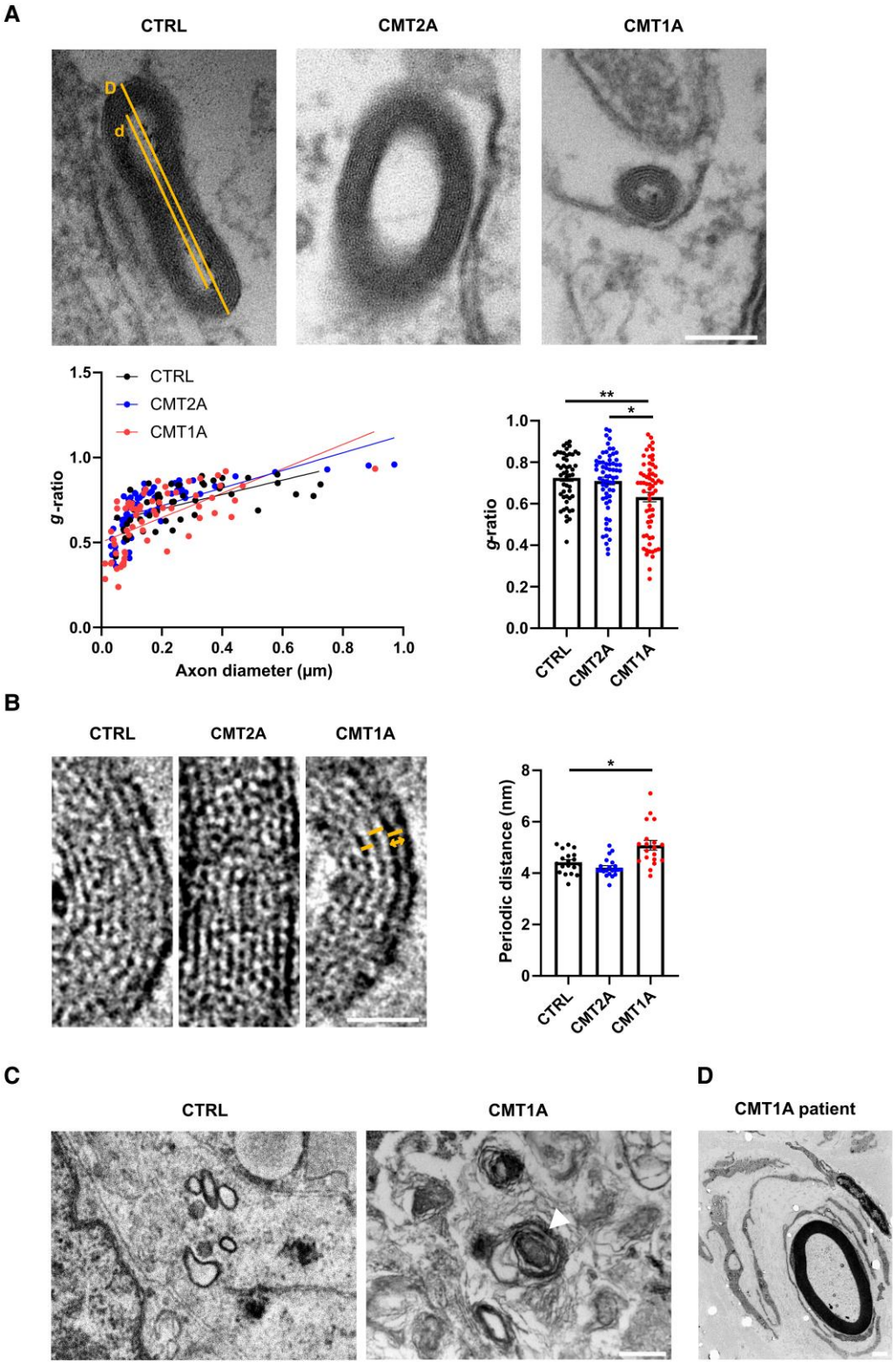

Figure 3 CMT1A-derived organoids cause myelin alterations. (**A**) TEM images at Day 25 showing myelination. Quantification of *g*-ratio (=*d*/*D*) was performed by measuring the axon and fibre diameter along the major axis ($n = 49–64$). Each dot represents individual myelinated neurons (data pooled from three independent differentiations; mean ± SEM). Scale bar = 100 nm. (**B**) TEM images at Day 25 of myelin sheath morphology. The images were obtained using a Fourier transform bandpass filter. Quantification of myelin periodic line distance ($n = 19–21$). Each dot represents the average value of measured myelin periodic line distances per myelinated neuron (data pooled from three independent differentiations; mean ± SEM). Scale bar = 25 nm. (**C**) Electron micrograph showing onion-bulb-like formation (arrowhead) in the CMT1A patient line at Day 50. Scale bar = 500 nm. (**D**) Electron micrograph of a post-mortem sural nerve biopsy in a 73-year-old CMT1A patient showing onion-bulb formation around a myelinated axon (EM end-magnification ×12 300). Statistical significance to evaluate *g*-ratio was performed using one-way ANOVA followed by Tukey's multiple comparisons test, while Kruskal–Wallis test with Dunn's multiple comparison was used to perform statistics on the myelin periodic line distance (*$P < 0.05$, **$P < 0.01$, ***$P < 0.001$, ****$P < 0.0001$).

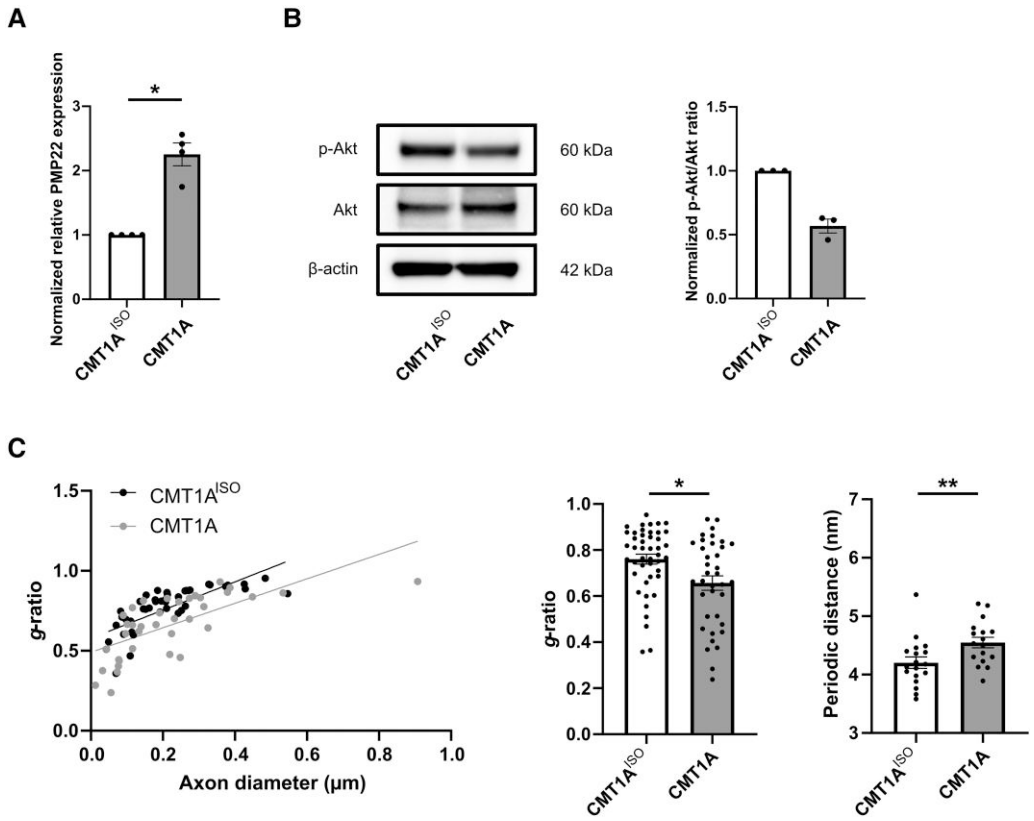

Figure 4 The CMT1A disease phenotype in iPSC-derived organoids is rescued in isogenic control line. (**A**) RT-qPCR to investigate the relative expression of PMP22 in iPSC-derived organoids at Day 25 ($n = 4$; data pooled from two independent differentiations; mean ± SEM). (**B**) p-Akt, Akt and β-actin levels at Day 25 in iPSC-derived organoids determined using western blot (*left*). Corresponding quantifications of normalized protein levels (*right*) ($n = 3$). (**C**) TEM experiments. *g*-ratio relative to axon diameter (*left*). Quantification of *g*-ratio (*middle*) ($n = 37$–45). Each dot represents individual myelinated neurons (data pooled from two independent differentiations; mean ± SEM). Quantification of myelin periodic line distance (*right*) ($n = 17$–18). Each dot represents the average value of measured myelin periodic line distances per myelinated neuron (data pooled from two independent differentiations; mean ± SEM). Statistical significance to evaluate *PMP22* expression, protein quantifications, *g*-ratio and myelin periodic line distance was performed using the Mann–Whitney U-test (*$P < 0.05$, **$P < 0.01$, ***$P < 0.001$, ****$P < 0.0001$).

To assess whether the correction of the PMP22-duplication rescues the early ultrastructural myelin alterations, we determined the *g*-ratio and myelin periodic distance at Day 25. We found that the isogenic CMT1A^{ISO} organoids significantly increased the *g*-ratio, restoring small hypermyelinated axons (Fig. 4C). In addition, the myelin compaction was likewise corrected in the iPSC-derived CMT1A^{ISO} organoids (Fig. 4C). In summary, the isogenic CMT1A^{ISO} line restored the disease phenotype of the CMT1A patient line, demonstrating that our results in iPSC-derived organoids are true hallmarks of CMT1A.

Short-hairpin RNA and combinatorial drug treatment downregulate *PMP22* expression and ameliorate the phenotype in CMT1A organoids

Since increased PMP22 gene dosage causes peripheral nerve dysmyelination in CMT1A, we investigated whether we could lower *PMP22* expression. This strategy already showed promising results in rodent models for CMT1A subjected to ASO treatments[15,17,32] and is currently also in clinical trial Phase III for the synergistic PXT3003 therapy (composed of three individual drugs; baclofen, naltrexone and sorbitol), which inhibits PMP22 expression levels.[13,14] So far, none of these promising therapies have been formally tested in human *in vitro* models due to the lack of an appropriate model system. To investigate whether the organoid model can be used to study the effects of *PMP22* reduction, organoids were treated with a combinatorial drug (containing a mixture of baclofen, naltrexone hydrochloride and D-sorbitol) or shRNAs.

We treated organoids from Day 6 onwards with a combination of baclofen, naltrexone hydrochloride and D-sorbitol. Note that this self-mixed combinatorial drug may deviate from what is currently being evaluated in the clinic. We used slightly adapted synergistic individual drug concentrations from the previously reported concentrations for neuron-Schwann cell co-cultures with dorsal root ganglia from CMT1A transgenic rats.[14] For the genetic approach, we used shRNAs to reduce *PMP22* expression. Two independent shRNAs (shRNA-1 and shRNA-2) were used to transduce organoids at Day 7 with either a high- or a low-dose, along with a control scramble shRNA (Supplementary Tables 4 and 5).

Combinatorial drug and shRNA-treated organoids were collected at Day 25, and *PMP22* expression was measured aiming for a ∼30–50% reduction, which has been shown to be beneficial to reverse CMT1A disease phenotypes in rodents.[15,17] Of note, we did not want to reduce the expression by >50%, as overreduction would result in the development of hereditary neuropathy with liability to pressure palsies, a disease known to produce marked myelin deficits in peripheral nerve biopsies.[33] Our shRNAs and combinatorial drug treatment successfully lowered *PMP22* expression (Fig. 5A and C). None of the treatments had a significant impact on the expression of *MPZ/P0*, a structural protein of compact myelin in the

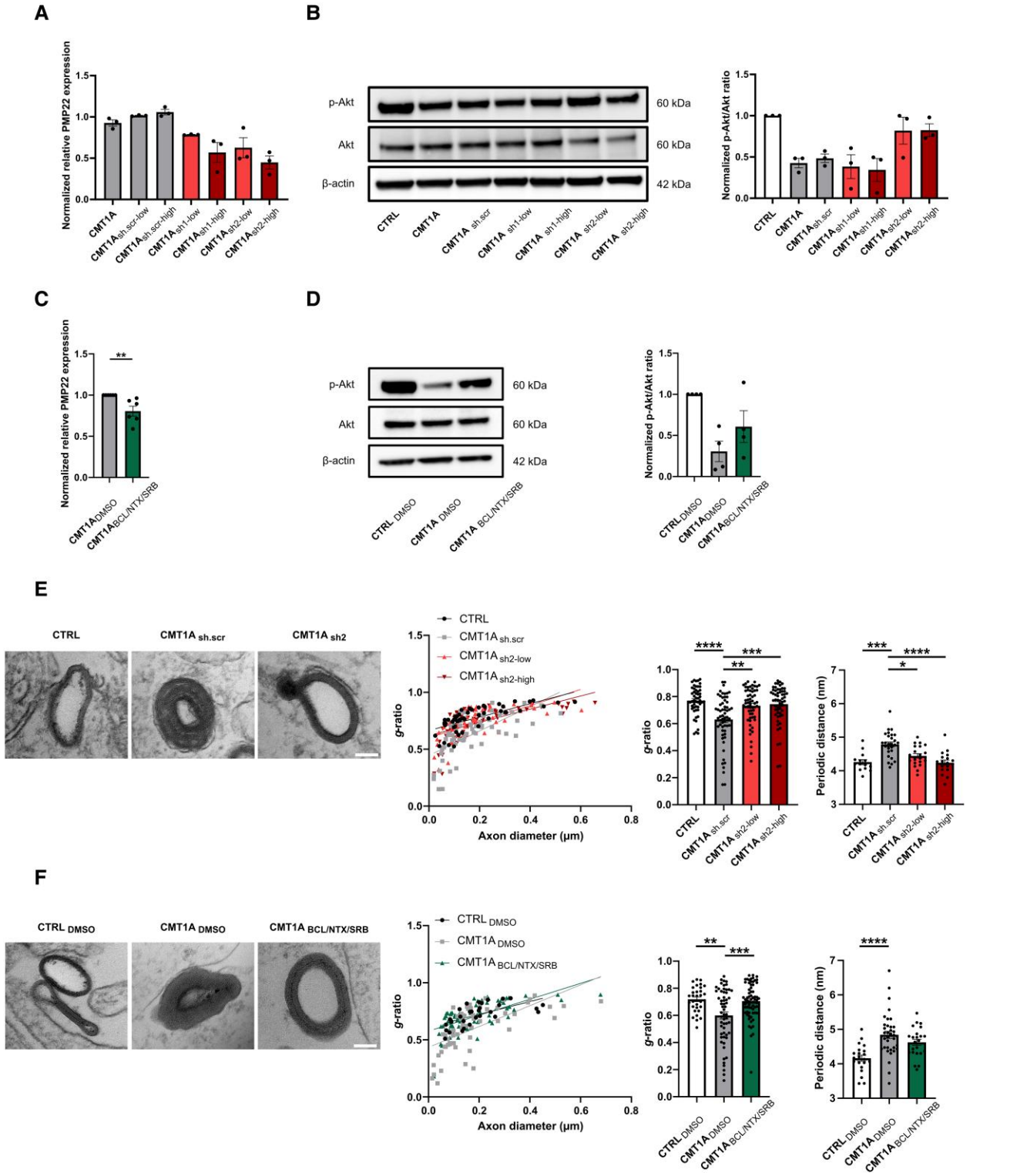

Figure 5 Pathological improvements after *PMP22* reduction in CMT1A-organoids. (**A**) RT-qPCR to investigate the relative expression of *PMP22* in iPSC-derived organoids after shRNA treatment at Day 25 ($n = 3$; data pooled from two independent differentiations; mean ± SEM). (**B**) p-Akt, Akt and β-actin levels at Day 25 in iPSC-derived organoids determined using western blot (*left*). Corresponding quantifications of normalized protein levels (*right*) ($n = 3$). (**C**) RT-qPCR to investigate the relative expression of *PMP22* in iPSC-derived organoids after combinatorial drug treatment at Day 25 ($n = 6$; data pooled from three independent differentiations; mean ± SEM). (**D**) p-Akt, Akt and β-actin levels at Day 25 in iPSC-derived organoids determined using western blot (*left*). Corresponding quantifications of normalized protein levels (*right*) ($n = 4$). (**E**) Representative TEM images of the smallest axons at Day 25 showing myelination after shRNA treatment (*left*). *g*-ratio relative to axon diameter (*middle*). Quantification of *g*-ratio (*right*) ($n = 51$–60). Each dot represents individual myelinated neurons (data pooled from two independent differentiations; mean ± SEM). Scale bar = 100 nm. Quantification of myelin periodic line distance (*right*) ($n = 14$–27). Each dot represents the average value of measured myelin periodic line distances per myelinated neuron (data pooled from two independent differentiations; mean ± SEM). (**F**) Representative TEM images of the smallest axons at

(Continued)

PNS,[34] underscoring the specificity of both therapeutic strategies (Supplementary Fig. 4B and C).

We verified whether the treatments could also restore p-Akt/Akt ratios. This revealed that the reduced p-Akt/Akt ratio could be reversed by shRNA-2 as well as by combinatorial drug supplementation, but not by shRNA-1 (Fig. 5B and D). On the basis of these results, we proceeded with shRNA-2 and the drug cocktail.

To assess whether lowered *PMP22* expression could also ameliorate ultrastructural myelin defects in the CMT1A organoids, we determined the *g*-ratio and myelin periodic distance upon combinatorial drug and shRNA-2 treatment. We found that both treatments significantly increased the *g*-ratio and particularly eliminated small hypermyelinated axons in CMT1A organoids (Fig. 5E and F). The low concentration of shRNA-2 and combinatorial drug treatment partially improved myelin compaction, whereas the high concentration of shRNA-2 was most effective and restored the myelin periodic line distance back to control levels (Fig. 5E and F). Together, this demonstrates that our complex human organoid model can recapitulate CMT1A disease features, which are ameliorated on reduction of *PMP22* expression by shRNAs or by pharmacological treatment.

Discussion

While multiple human CNS organoid models have been established,[35] for example to study microcephaly,[36] organoids focusing on the PNS have been unexplored. In this study, a complex organoid culture that mimics the human PNS in its cellular content and basic structure was generated. The organoids are composed of multiple self-organizing and interacting cell types, including myelinating Schwann cells. Using these organoids, we studied CMT1A, a hereditary peripheral neuropathy specifically affecting the myelination of peripheral nerves. Patient-derived CMT1A iPSCs demonstrated on differentiation that the organoid model recapitulates many of the early disease hallmarks. Moreover, our study provides the first evidence in a human system that combined treatment with baclofen, naltrexone and sorbitol (compounds being part of PXT3003) can ameliorate pathological features of CMT1A neuropathy. Of note, the bioavailability of these compounds may be different in the organoid model compared to the availability in distal parts of a human peripheral nerve. A rescue in myelin deficits was also confirmed when using a shRNA molecule directed towards reducing *PMP22* gene expression in the CMT1A organoid system.

A wide range of inherited and acquired PNS pathologies are characterized by myelination defects. Previous efforts in modelling such diseases *in vitro* have been limited to the use of 2D co-cultures that were of non-human origin.[11] The modelling of neuropathies in organoid cultures may offer new insights into the early stages of disease and become relevant to validate therapeutic molecules. The iPSC-derived organoids containing myelinating Schwann cells would also allow studying other neuropathies affecting Schwann cells, such as Guillain–Barré syndrome, chronic inflammatory demyelinating polyneuropathy or schwannomatosis. In addition, bacterial pathogens such as *Mycobacterium leprae* causing leprosy, are known to invade peripheral nerves and grow within Schwann cells.[37] Infecting organoid cultures with *M. leprae* would offer the possibility to obtain insights into the invasion in Schwann cells.

Although organoids offer a model that closely mimics the *in vivo* complexity, composed of many different cell types, this *in vitro* model provides no directional cell growth. This differs from the *in vivo* situation, where the PNS stretches in a directional manner from the spinal cord towards the most distal parts, making it challenging to perform NMJ-focused studies as they could be located throughout the organoid. For this reason, 2D models will remain useful to address focused questions. Microfluidic chambers allow directional growth of motor neurons towards muscle-containing chambers that provide clustering of NMJs. This, from a technical perspective, facilitates experiments in which a sufficient number of NMJs would need to be screened.

Further improvements of the organoid model could focus on these shortcomings. As described in neuromuscular organoids[22] or neural-muscle assembloids,[38] separating neural and muscle compartments provide more directional growth from the motor neuron towards muscle, facilitating certain experiments. A second improvement would be to also investigate additional developmental stages in the myelin architecture in organoids or assembloids.

Another exciting opportunity for this model is the possibility to study the role of PNS macrophages that are involved in nerve repair after injury, by phagocytosing myelin debris.[39,40] In some CMT disease subtypes, macrophages can also adopt pathogenic functions under distinct conditions, especially when activated in unlesioned nerves.[41,42] Cytokine CSF-1 was identified as a key molecule in the activation of nerve macrophages. Targeting the CSF-1 receptor using an inhibitor, was shown to substantially improve the disease course in CMT1B and CMT1X mouse models underscoring the pathogenic role of macrophages. If we aim to study the role of peripheral immune cell infiltrations in the future, one could adapt the model or create autologous co-cultures of nerve macrophages and iPSC-derived organoids of CMT patients and isogenic and unrelated controls.

In summary, our study highlights the potential to study demyelinating diseases of the PNS in human-derived organoids and provides additional support for PMP22 expression inhibitors as a promising therapeutic approach for CMT1A.

Acknowledgements

The authors thank the patients and control individuals who volunteered to provide skin biopsies to generate iPSC lines for research purposes through informed consent. We obtained the iPSC line CS67iCMT from Cedars-Sinai Biomanufacturing Center iPSC Core Repository. We thank Professor Jean-Pierre Timmermans, Dr Isabel Pintelon, Ms Karen Sterck, Ms Sofie Thys and Ms Elien Theuns (Antwerp Centre for Advanced Microscopy) and Ms Inge Bats (Institute Born-Bunge) for assistance with electron microscopy.

Figure 5 Continued
Day 25 showing myelination after combinatorial drug treatment (left). *g*-ratio relative to axon diameter (*middle*). Quantification of *g*-ratio (*right*) ($n = 31$–66). Each dot represents individual myelinated neurons (data pooled from two independent differentiations; mean ± SEM). Scale bar = 100 nm. Quantification of myelin periodic line distance (*right*) ($n = 21$–37). Each dot represents the average value of measured myelin periodic line distances per myelinated neuron (data pooled from two independent differentiations; mean ± SEM). Statistical significance to evaluate *g*-ratio was performed using one-way ANOVA followed by Tukey's multiple comparisons test, while Kruskal–Wallis test with Dunn's multiple comparison was used to perform statistics on the myelin periodic line distance and protein quantifications. Mann–Whitney U-test was used to test significance of *PMP22* expression on combinatorial drug treatment (*$P < 0.05$, **$P < 0.01$, ***$P < 0.001$, ****$P < 0.0001$).

Funding

This work was supported in part by the University of Antwerp (DOC-PRO4 PhD fellowship to J.V.L. and TOP-BOF research grant no. 38694 to V.T.) and the Association Française contre les Myopathies (AFM research grant no. 24063). The Tecnai G2 Spirit BioTWIN TEM was purchased with support of the Hercules Foundation (Hercules Type 2: AUHA004). The multi-well MEA was supported by FWO infrastructure grant no. 41425. L.V. is supported by a PhD fellowship of the Flanders Fund for Scientific Research (FWO-Flanders). E.A. is a postdoctoral fellow of the FWO-Flanders (Fellowship 1228021N). J.B. is supported by a Senior Clinical Researcher mandate of the FWO-Flanders under grant agreement number 1805021N. J.B. is a member of the European Reference Network for Rare Neuromuscular Diseases (ERN EURO-NMD). S.W., J.B. and V.T. are members of the µNeuro Center of Excellence at the University of Antwerp.

Competing interests

The authors declare no competing interests, as well as no relationship with Pharnext.

Supplementary material

Supplementary material is available at *Brain* online.

References

1. Saporta MA, Shy ME. Inherited peripheral neuropathies. *Neurol Clin*. 2013;31:597-619.
2. Raeymaekers P, Timmerman V, Nelis E, *et al*. Duplication in chromosome 17p11.2 in Charcot-Marie-Tooth neuropathy type 1a (CMT 1a). the HMSN collaborative research group. *Neuromuscul Disord*. 1991;1:93-97.
3. Lupski JR, de Oca-Luna RM, Slaugenhaupt S, *et al*. DNA duplication associated with Charcot-Marie-Tooth disease type 1A. *Cell*. 1991;66:219-232.
4. Timmerman V, Nelis E, Van Hul W, *et al*. The peripheral myelin protein gene PMP-22 is contained within the Charcot-Marie-Tooth disease type 1A duplication. *Nat Genet*. 1992;1:171-175.
5. Thomas PK. Overview of Charcot-Marie-Tooth disease type 1A. *Ann N Y Acad Sci*. 1999;883:1-5.
6. Gibbs RM, Lipnick S, Bateman JW, *et al*. Toward precision medicine for neurological and neuropsychiatric disorders. *Cell Stem Cell*. 2018;23:21-24.
7. Park I-H, Arora N, Huo H, *et al*. Disease-specific induced pluripotent stem cells. *Cell*. 2008;134:877-886.
8. Van Lent J, Verstraelen P, Asselbergh B, *et al*. Induced pluripotent stem cell-derived motor neurons of CMT type 2 patients reveal progressive mitochondrial dysfunction. *Brain*. 2021;144:2471-2485.
9. Saporta MA, Dang V, Volfson D, *et al*. Axonal Charcot-Marie-Tooth disease patient-derived motor neurons demonstrate disease-specific phenotypes including abnormal electrophysiological properties. *Exp Neurol*. 2015;263:190-199.
10. Perez-Siles G, Cutrupi A, Ellis M, *et al*. Energy metabolism and mitochondrial defects in X-linked Charcot-Marie-Tooth (CMTX6) iPSC-derived motor neurons with the p.R158H PDK3 mutation. *Sci Rep*. 2020;10:9262.
11. Clark AJ, Kaller MS, Galino J, *et al*. Co-cultures with stem cell-derived human sensory neurons reveal regulators of peripheral myelination. *Brain*. 2017;140:898-913.
12. Liu Q, Spusta SC, Mi R, *et al*. Human neural crest stem cells derived from human ESCs and induced pluripotent stem cells: Induction, maintenance, and differentiation into functional Schwann cells. *Stem Cells Transl Med*. 2012;1:266-278.
13. Prukop T, Stenzel J, Wernick S, *et al*. Early short-term PXT3003 combinational therapy delays disease onset in a transgenic rat model of Charcot-Marie-Tooth disease 1A (CMT1A). *PLoS ONE*. 2019;14:e0209752.
14. Chumakov I, Milet A, Cholet N, *et al*. Polytherapy with a combination of three repurposed drugs (PXT3003) down-regulates Pmp22 over-expression and improves myelination, axonal and functional parameters in models of CMT1A neuropathy. *Orphanet J Rare Dis*. 2014;9:201.
15. Zhao HT, Damle S, Ikeda-Lee K, *et al*. PMP22 antisense oligonucleotides reverse Charcot-Marie-Tooth disease type 1A features in rodent models. *J Clin Invest*. 2018;128:359-368.
16. Stavrou M, Kagiava A, Choudury SG, *et al*. A translatable RNAi-driven gene therapy silences PMP22/Pmp22 genes and improves neuropathy in CMT1A mice. *J Clin Invest*. 2022;132:e159814.
17. Boutary S, Caillaud M, El Madani M, *et al*. Squalenoyl siRNA PMP22 nanoparticles are effective in treating mouse models of Charcot-Marie-Tooth disease type 1 A. *Commun Biol*. 2021;4:317.
18. Pereira JD, DuBreuil DM, Devlin AC, *et al*. Human sensorimotor organoids derived from healthy and amyotrophic lateral sclerosis stem cells form neuromuscular junctions. *Nat Commun*. 2021;12:4744.
19. Schneider CA, Rasband WS, Eliceiri KW. NIH image to ImageJ: 25 years of image analysis. *Nat Methods*. 2012;9:671-675.
20. Schindelin J, Arganda-Carreras I, Frise E, *et al*. Fiji: An open-source platform for biological-image analysis. *Nat Methods*. 2012;9:676-682.
21. Gouti M, Delile J, Stamataki D, *et al*. A gene regulatory network balances neural and mesoderm specification during vertebrate trunk development. *Dev Cell*. 2017;41:243-261.e7.
22. Faustino Martins JM, Fischer C, Urzi A, *et al*. Self-organizing 3D human trunk neuromuscular organoids. *Cell Stem Cell*. 2020;27:498.
23. Hutchins EJ, Bronner ME. Draxin acts as a molecular rheostat of canonical Wnt signaling to control cranial neural crest EMT. *J Cell Biol*. 2018;217:3683-3697.
24. Ashique AM, Choe Y, Karlen M, *et al*. The Rfx4 transcription factor modulates shh signaling by regional control of ciliogenesis. *Sci Signal*. 2009;2:ra70.
25. Liu Q, Yuan B, Lo KA, *et al*. Adiponectin regulates expression of hepatic genes critical for glucose and lipid metabolism. *Proc Natl Acad Sci U S A*. 2012;109:14568-14573.
26. Liu Z, Jin YQ, Chen L, *et al*. Specific marker expression and cell state of Schwann cells during culture in vitro. *PLoS ONE*. 2015;10:e0123278.
27. Wolbert J, Li X, Heming M, *et al*. Redefining the heterogeneity of peripheral nerve cells in health and autoimmunity. *Proc Natl Acad Sci U S A*. 2020;117:9466-9476.
28. Shimba K, Asahina T, Sakai K, Kotani K, Jimbo Y. Recording saltatory conduction along sensory axons using a high-density microelectrode array. *Front Neurosci*. 2022;16:854637.
29. Nobbio L, Mancardi G, Grandis M, *et al*. PMP22 transgenic dorsal root ganglia cultures show myelin abnormalities similar to those of human CMT1A. *Ann Neurol*. 2001;50:47-55.
30. Mukherjee-Clavin B, Mi R, Kern B, *et al*. Comparison of three congruent patient-specific cell types for the modelling of a

human genetic Schwann-cell disorder. *Nat Biomed Eng*. 2019;3: 571-582.
31. Fledrich R, Stassart RM, Klink A, *et al*. Soluble neuregulin-1 modulates disease pathogenesis in rodent models of Charcot-Marie-Tooth disease 1A. *Nat Med*. 2014;20:1055-1061.
32. Gautier B, Hajjar H, Soares S, *et al*. AAV2/9-mediated silencing of PMP22 prevents the development of pathological features in a rat model of Charcot-Marie-Tooth disease 1A. *Nat Commun*. 2021;12:2356.
33. Gabriel JM, Erne B, Pareyson D, *et al*. Gene dosage effects in hereditary peripheral neuropathy. Expression of peripheral myelin protein 22 in Charcot-Marie-Tooth disease type 1A and hereditary neuropathy with liability to pressure palsies nerve biopsies. *Neurology*. 1997;49:1635-1640.
34. Otani Y, Ohno N, Cui J, *et al*. Upregulation of large myelin protein zero leads to Charcot-Marie-Tooth disease-like neuropathy in mice. *Commun Biol*. 2020;3:121.
35. Amin ND, Paşca SP. Building models of brain disorders with three-dimensional organoids. *Neuron*. 2018;100:389-405.
36. Lancaster MA, Renner M, Martin CA, *et al*. Cerebral organoids model human brain development and microcephaly. *Nature*. 2013;501:373-379.
37. Alves L, de Mendonça Lima L, da Silva Maeda E, *et al*. *Mycobacterium leprae* infection of human Schwann cells depends on selective host kinases and pathogen-modulated endocytic pathways. *FEMS Microbiol Lett*. 2004;238:429-437.
38. Andersen J, Revah O, Miura Y, *et al*. Generation of functional human 3D cortico-motor assembloids. *Cell*. 2020;183: 1913-1929.e26.
39. Ydens E, Cauwels A, Asselbergh B, *et al*. Acute injury in the peripheral nervous system triggers an alternative macrophage response. *J Neuroinflammation*. 2012;9:176.
40. Ydens E, Amann L, Asselbergh B, *et al*. Profiling peripheral nerve macrophages reveals two macrophage subsets with distinct localization, transcriptome and response to injury. *Nat Neurosci*. 2020;23:676-689.
41. Klein D, Patzkó Á, Schreiber D, *et al*. Targeting the colony stimulating factor 1 receptor alleviates two forms of Charcot-Marie-Tooth disease in mice. *Brain*. 2015;138(Pt 11): 3193-3205.
42. Klein D, Groh J, Yuan X, *et al*. Early targeting of endoneurial macrophages alleviates the neuropathy and affects abnormal Schwann cell differentiation in a mouse model of Charcot-Marie-Tooth 1A. *Glia*. 2022;70:1100-1116.